Journal of Molecular Catalysis A: Chemical 326 (2010) 41–47

Contents lists available at ScienceDirect

Journal of Molecular Catalysis A: Chemical

journal homepage: www.elsevier.com/locate/molcata

A DFT study on the reaction mechanisms of ketene–ketone [2 + 2 + 2] cycloaddition to form 3-aryglutaric anhydrides under a Lewis acid catalysis: What is the role of BF_3?

Donghui Wei, Wenjing Zhang, Yanyan Zhu*, Mingsheng Tang*

Department of Chemistry, Center of Computational Chemistry, Zhengzhou University, DAXUE Road 75 #, Zhengzhou, Henan 450052, China

ARTICLE INFO

Article history:
Received 24 February 2010
Received in revised form 8 April 2010
Accepted 8 April 2010
Available online 4 May 2010

Keywords:
Density functional theory (DFT)
Ketene–ketone cycloaddition
Frontier molecular orbital
Lewis acid

ABSTRACT

The mechanisms of the title reaction have been studied by density functional theory (DFT). Three possible reaction channels, including one non-catalyzed channel (channel 1) and two channels promoted by Lewis acid BF_3 (channels 2 and 3) are shown. The calculated results indicate that one of the catalyzed channels (channel 2) is most energy favorable among all the three channels, so it occurs more often than others. To the best of our knowledge, why Lewis acids can lower the energy barrier of ketene–ketone cycloaddition largely has still been ambiguous by now. In order to clarify the puzzle, we have used an effective method of frontier molecular orbital (FMO) analysis to explain how the Lewis acid BF_3 make the reaction easier to occur. The results revealed that in addition to the orbital symmetries and the energy gaps between the frontier molecular orbitals, the different overlap modes of the frontier molecular orbitals are also important for the reaction in this paper.

1. Introduction

Desymmetrization of meso- and prochiral compounds is a powerful approach in asymmetric synthesis [1]. Due to the wide application of this approach [2–5], the new synthetic methodologies of 3-aryglutaric anhydrides have attracted more and more attention. For example, 3-aryglutaric acids have been synthesized by condensation of arylaldehydes with two molecules of ethyl acetoacetate followed by deacetylation and hydrolysis of ester groups by strong base [6]. Recently, a one-pot synthesis of 3-aryglutaric acids has been reported [7]. In this method, bis-isoxazole derivatives formed from 3,5-dimethyl-4-nitroisoxazole and arylaldehydes are oxidized in situ to the dicarboxylic acids by $KMnO_4$. Glutaric anhydrides are obtained by treatment of glutaric acids with acetic anhydride. Moreover, Matsunaga et al. have reported the first one-pot synthesis of 3-aryl- or 3-alkyl-3-arylglutaric anhydrides by reaction of ketene with benzaldehydes or acetophenones under a Lewis acid catalysis (Scheme 1) [8], which is a very convenient method and has been widely used to form β-lactones (**M1**, Scheme 1) in the experiments [9–18].

Although there have been several computational papers investigating the mechanisms of ketene–ketone [2 + 2] cycloaddition to form β-lactones [19,20], to the best of our knowledge, why Lewis acids can lower the energy barrier largely is still mysterious. For example, Cossio et al. reported ab initio calculations on catalyst (BH_3), substituents, and solvent (CH_2Cl_2) effects on the reaction between ketene (or chloroketene) and formaldehyde (or acetaldehyde) [19b,19c]. However, they did not give a deep investigation on the frontier molecular orbital interaction, which should be very important for the cycloaddition reaction. In addition, Rajzmann and co-workers had compared two reaction paths on formation of β-lactones under non-catalysis condition (Scheme 2) [20a], and through Lewis acid-promoted [2 + 2] cycloaddition (Scheme 3) using semiempirical (AM1/RHF and AM1/CI) and ab initio (HF/6-31G* and MP2/6-31G*) calculations [20b]. They thought that BF_3 had a greater influence on the activation energy of path A compared to path B. Consequently, path A, which is unfavored in the uncatalyzed reaction (A vs B: 38 vs 32 kcal/mol, Scheme 2) [20a], becomes favored in the BF_3-catalyzed one (A vs B: 14 vs 24 kcal/mol, Scheme 3). And the IRC results of path A can only lead to **MA1** (Scheme 3) rather than **MA2** (Scheme 3) in the BH_3-catalyzed one, so they thought it is better to use BF_3 rather than BH_3 as a model Lewis acid in this reaction [20b]. Actually, we have validated the IRC calculation results of path A in Schemes 2 and 3, which suggests that the reaction cannot lead to the β-lactones under either non-catalysis orBX_3-catalyzed (X = H and F) conditions. The C(2) and C(3) atoms are close to each other when O(1) and C(4) atoms are far away from each other in the IRC results, and the structure of intermediate such as **MA** (Scheme 3) cannot be localized, but there were not convincing evidences reported to disaffirm this path, so it has still been the controversial land by now.

* Corresponding authors. Tel.: +86 371 67767051; fax: +86 371 67767051.
E-mail addresses: zhuyan@zzu.edu.cn (Y. Zhu), mstang@zzu.edu.cn (M. Tang).

1381-1169/$ – see front matter © 2010 Elsevier B.V. All rights reserved.
doi:10.1016/j.molcata.2010.04.005

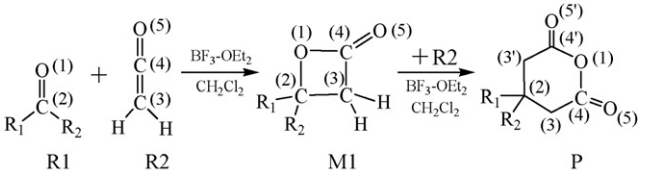

Scheme 1. The scheme of the title reaction.

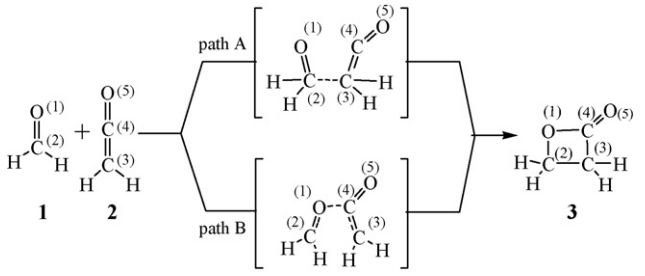

Scheme 2. Two reaction paths toward β-lactone under non-catalysis: path A vs path B [20a].

Noteworthy, Yamabe et al. had provided the precise frontier molecular orbital (FMO) pictures for the [2 + 2] cycloaddition under non-catalysis by the IRC of path B in Scheme 2 [19d,19e], but it is still unknown whether there is a same overlap mode of the frontier molecular orbitals under the Lewis acid catalysis in the past decades. All of the above works prompted us not only to investigate the mechanisms of the title reaction, but also to give a deep investigation on the frontier molecular orbital interactions. We think this work should confirm how the Lewis acid works and what the role of BF_3 is, which should be certainly helpful for the new catalyzed reaction designs.

In this project, the reaction of acetophenone (**R1**, Scheme 4) with ketene (**R2**, Scheme 4) under Lewis acid (BF_3-OEt_2) catalysis, which mainly generates 4-methyl-4-phenyl-dihydro-3H-pyran-2,6-dione (**P**, Scheme 4) in CH_2Cl_2 solvent, has been chosen as the object of investigation. Because the energy differences between *R* and *S* configurations of C(2) atom are so tiny, and the products **P1**, **P2** and **P** are not chiral compounds, so all the chiral structures in Scheme 4 are discussed in the *S* configuration. The reaction mechanisms have been studied using density functional theory (DFT), which has been widely used in the study of mechanism [21,22].

2. Computational details

The geometries of the reactants, transition states, intermediates and products in all reaction channels were optimized at the B3LYP/6-31G (d, p) [23–25] level in CH_2Cl_2 solvent, using the integral equation formalism polarizable continuum model (IEF-PCM) method [26,27]. The corresponding vibrational frequencies were calculated at the same level to take account of the zero-point vibrational energy (ZPVE) and to identify the transition states. At the same time, the structures of intermediates and the transition states were confirmed by using the intrinsic reaction coordinate (IRC) [28,29]. All the theoretical calculations were performed using the Gaussian 03 [30] suits of programs.

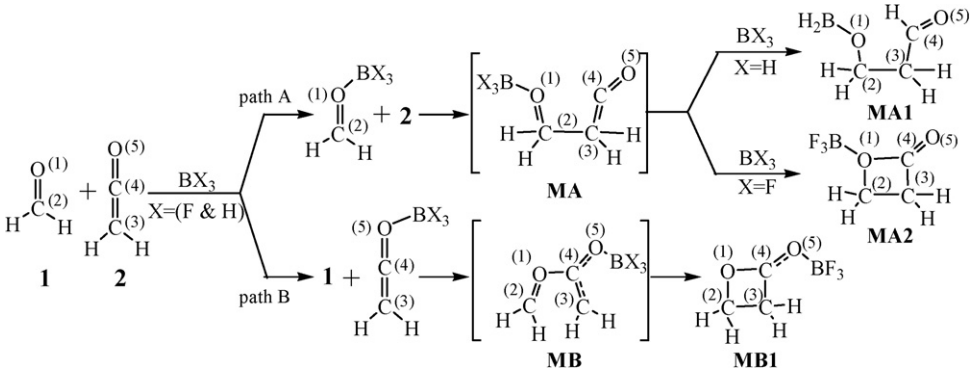

Scheme 3. Two reaction paths on formation of β-lactones through Lewis acid-promoted [2 + 2] cycloaddition: path A vs path B [20b].

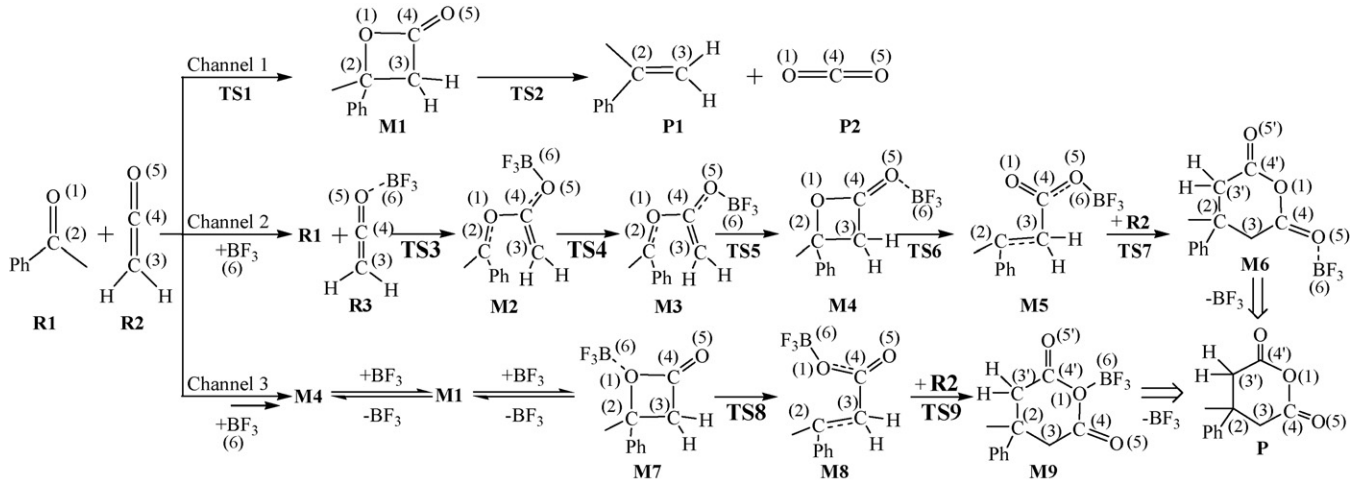

Scheme 4. The three possible reaction channels.

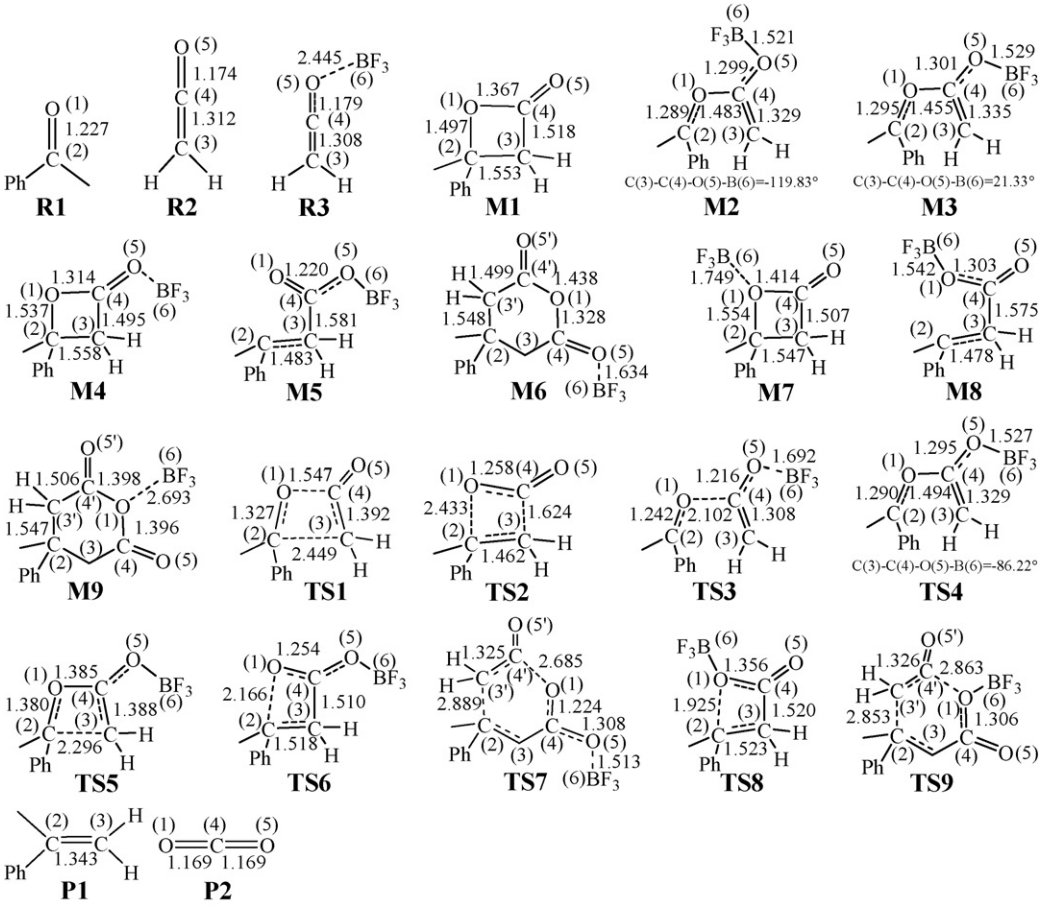

Fig. 1. The structures and the geometrical parameters of the reactants, intermediates, products and transition states optimized at the B3LYP/6-31G (d, p) level in CH_2Cl_2 solvent (bond length in Å, dihedral angle in°).

3. Results and discussion

3.1. The three possible reaction channels

Based on the experimental results, in this paper, we have suggested three possible reaction channels to lead to three different products (Scheme 4). Fig. 1 presents the structures and geometrical parameters of all the reactants, intermediates, transition states and products. We set the energies (E + ZPVE) of **R1** + **R2** + **R3** as 0.0 kcal/mol as reference in the potential energy profiles (Figs. 2–4). The products of channel 1 are **P1** and **P2** (Scheme 4) while the product of channels 2 and 3 is **P**. The processes could be illustrated as follows.

3.1.1. Reaction channel 1

As shown in Scheme 4, there are two steps in the reaction channel 1. Firstly, **R1** reacts with **R2** to form a four-membered ring (O(1)–C(2)–C(3)–C(4)) intermediate **M1** through a [2 + 2] cycloaddition via **TS1**. Next, the four-membered ring opens to generate the product **P1** and **P2** via **TS2**. During the ring-forming step, two double-bonds (O(1)–C(2), C(3)–C(4)) become the single-bonds, and two new single-bonds (O(1)–C(4), C(2)–C(3)) form. In other words, there are two Π bonds break so as to generate two new σ bonds. With our calculated results, this process is a concerted reaction. Then in the ring-opening step, two single-bonds (O(1)–C(2), C(3)–C(4)) break while two new double-bonds (O(1)–C(4), C(2)–C(3)) form, which is also a concerted reaction.

It can be observed from Fig. 1 that the distances of the O(1)–C(2), C(2)–C(3), C(3)–C(4) and O(1)–C(4) are 1.327 Å, 2.449 Å, 1.392 Å and 1.547 Å in **TS1**, and these distances change from 1.497 Å, 1.553 Å, 1.518 Å and 1.367 Å in **M1** to 2.433 Å, 1.462 Å, 1.624 Å and 1.258 Å in **TS2**, respectively. The energy barrier of ring-forming process is 28.4 kcal/mol and that of ring-opening process is 21.6 kcal/mol at B3LYP/6-31G (d, p) level in CH_2Cl_2 solvent (Fig. 2), this fact explains why the reaction is not easy to process at room temperature.

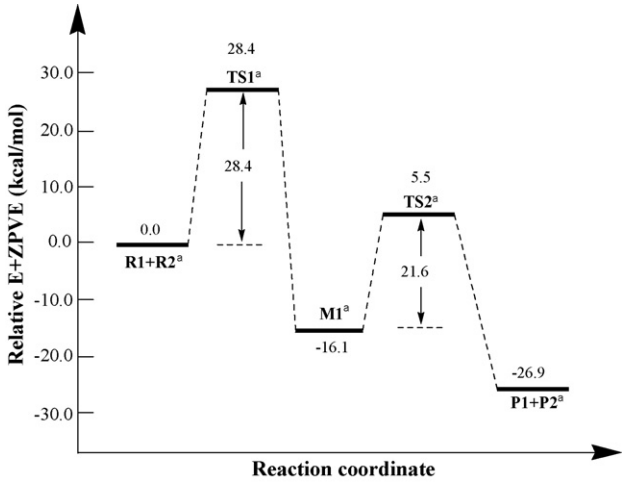

Fig. 2. The energy profile of channel 1 (unit: kcal/mol, the superscript a represents adding the energy of **R3**).

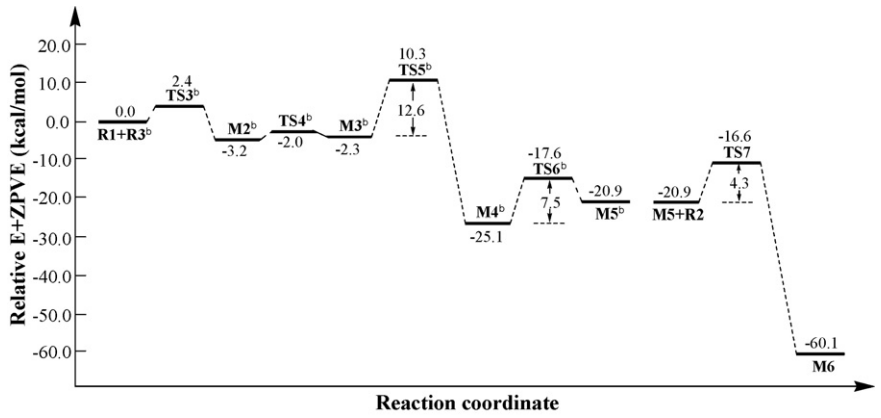

Fig. 3. The energy profile of channel 2 (unit: kcal/mol, the superscript b represents adding the energy of **R2**).

3.1.2. Reaction channel 2

As we can see from Scheme 4, the O(5) atom of **R2** has lone pair electrons, therefore, the O(5) atom can form a coordination bond with B(6) atom of Lewis acid BF_3, and **R2** may become **R3**. There are three processes in channel 2.

In the first process, **R1** reacts with **R3** to form the four-membered ring (O(1)–C(2)–C(3)–C(4)) by three stepwise reactions via **TS3**, **TS4** and **TS5**. The distance of O(1)–C(4) changes from 2.102 Å in **TS3** to 1.483 Å in **M2**, and the bond length of O(5)–B(6) changes from 1.692 Å in **TS3** to 1.521 Å in **M2**, which shows that the O(1)–C(4) bond generates via **TS3**. Then the dihedral angle C(3)–C(4)–O(5)–B(6) changes from −119.23° in **M2** to 21.33° in **M3** via **TS4**. At last, the C(2)–C(3) bond and the four-membered ring (O(1)–C(2)–C(3)–C(4)) intermediate generate via **TS5**. The bond lengths of O(1)–C(2), C(2)–C(3), C(3)–C(4) and O(1)–C(4) change from 1.380 Å, 2.296 Å, 1.388 Å and 1.385 Å in **TS5** to 1.537 Å, 1.558 Å, 1.495 Å and 1.314 Å in **M4**, respectively (Fig. 1). The highest energy barrier of this process is only 12.6 kcal/mol (Fig. 3), which is not a high barrier at room temperature.

At the second process, the four-membered ring opens to form the intermediate **M5** via **TS6**. In contrast to channel 1, the ring-opening process is also not a concerted reaction, and here only the single-bond O(1)–C(2) breaks. The bond lengths of O(1)–C(2), C(2)–C(3), C(3)–C(4) and O(1)–C(4) are 2.166 Å, 1.518 Å, 1.510 Å and 1.254 Å in **TS6**, respectively (Fig. 1). The energy barrier of this step is low (7.5 kcal/mol, Fig. 3) for the room temperature. Furthermore, from the structures of **M5** and **P**, we know that the intermediate **M5** is important for the formation of the main product **P**.

At the third process, **M5** reacts with another **R2** to form the intermediate **M6** via [4 + 2] transition state **TS7**. The distances of O(1)–C(4′), C(2)–C(3′) and C(3′)–C(4′) change from 2.685 Å, 2.889 Å and 1.325 Å in **TS7** to 1.438 Å, 1.548 Å and 1.499 Å in **M6**, respectively (Fig. 1). The energy barrier of the third process is very low (4.3 kcal/mol, Fig. 3) for the room temperature, and the energy of **M6** is 60.1 kcal/mol lower than the energy of **R1** + **R2** + **R3**, indicating that this step is an exothermic process and the intermediate **M6** can generate easily at room temperature. At last, the main product **P** can generate by separating BF_3 from **M6**. Noteworthy, the energy of **M6** is 33.2 kcal/mol lower than that of **P1** + **P2**[a] in Fig. 2, so the main product should be **P** rather than **P1** + **P2**, and it is useless to consider the CO_2 elimination in the catalyzed reaction channels.

3.1.3. Reaction channel 3

The reaction channel 3 is similar to path A in Scheme 3, we also consider the BF_3 may form a coordination bond with O(1) atom. However, our IRC results of the formation of four–membered ring transition state only can lead to an intermediate who is similar to **MA1** (Scheme 3) rather than **MA2** (Scheme 3). Based on what we have mentioned in the introduction, we think the path A in Scheme 3 is not a good reaction channel. And as can be seen from Scheme 4, there are also three steps in channel 3.

First, the process of forming the four-membered ring (O(1)–C(2)–C(3)–C(4)) intermediate **M4** is the same as the channel 2, then **M4** should convert to **M7** via **M1** by adsorption and desorption of BF_3. Because the energy of **M4** is 6.4 kcal/mol lower than that of **M7**, so we think the following processes should continue via **M4** rather than **M7**, which indicates that channel 2 should occur more often than channel 3. The bond lengths of O(1)–C(2), C(2)–C(3), C(3)–C(4) and O(1)–C(4) are 1.554 Å, 1.547 Å, 1.507 Å and 1.414 Å in **M7**, respectively (Fig. 1).

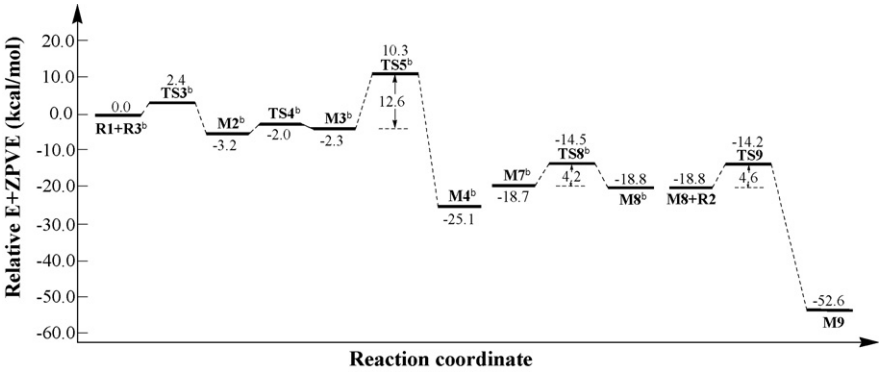

Fig. 4. The energy profile of channel 3 (unit: kcal/mol, the superscript b represents adding the energy of **R2**).

Second, the four-membered ring opens to form the intermediate **M8** via **TS8**. The bond lengths of O(1)–C(2), C(2)–C(3), C(3)–C(4) and O(1)–C(4) are 1.925 Å, 1.523 Å, 1.520 Å and 1.356 Å in **TS8**, respectively (Fig. 1). The energy barrier of this step is only 4.2 kcal/mol (Fig. 4). Furthermore, from the structures of **M8** and **P**, we know that the intermediate **M8** is as important as **M5** for the formation of the main product **P**.

Third, **M8** reacts with another **R2** to form the intermediate **M9** via [4+2] transition state **TS9**. The distances of O(1)–C(4′), C(2)–C(3′) and C(3′)–C(4′) change from 2.863 Å, 2.853 Å and 1.326 Å in **TS9** to 1.398 Å, 1.547 Å and 1.506 Å in **M9**, respectively (Fig. 1). Noteworthy, the distance of O(1)–B(6) is 2.693 Å, so the main product **P** can generate easily by separating BF_3 from **M9**. Nevertheless, the energy barrier of this step is 0.3 kcal/mol higher than that of channel 2, and the energy of **M9** is 7.5 kcal/mol higher than that of **M6**, which illuminates that channel 3 will be at a disadvantage in the competition, so the main product **P** should be obtained via **M6** rather than **M9**.

3.2. Frontier molecular orbital analysis

In all the three channels, the process of [2+2] cycloaddition has the highest energy barrier, which is lowered largely under the catalysis of BF_3, so the frontier molecular orbital (FMO) analysis should certainly be carried out to explain what the role of BF_3 is in this paper. As shown in Fig. 5, Yamabe and co-workers thought that the two one-centre frontier molecular orbital interactions took place independently in the [2+2] cycloaddition, the left interaction in Fig. 5 would lead to the formation of O(1)–C(4) σ orbital and the right interaction in Fig. 5 would lead to the formation of C(2)–C(3) σ orbital, and the two one-centre molecular orbital interactions are not concerned with orbital symmetries [19d].

In this paper, the two one-centre frontier molecular orbital interactions are between $LUMO_{R2}$ and $HOMO\text{-}1_{R1}$, $LUMO_{R1}$ and $HOMO_{R2}$, respectively. We have calculated the energy gaps of the two frontier molecular orbital interactions under non-catalysis or the catalysis of BF_3 in Fig. 6. The energy gap between $LUMO_{R2}$ and $HOMO\text{-}1_{R1}$ has become narrow, which demonstrates that the C(4)–O(1) bond will form more smoothly when using BF_3 as the catalyst. However, the energy gap between $LUMO_{R1}$ and $HOMO_{R2}$ has become wide rather than narrow under the catalysis of BF_3, which seems to be against with the above calculated results. In addition, for the interaction between $HOMO\text{-}1_{R1}$ and $LUMO_{R2}$ (or $LUMO_{R3}$) (which will form the O(1)–C(4) σ orbital), it is absolutely an one-centre frontier molecular orbital interaction, and this constructs a head to head "symmetry-matched" overlap mode. While for the interaction between $LUMO_{R1}$ and $HOMO_{R2}$ (or $HOMO_{R3}$), the head to head overlap mode seems "symmetry-forbidden" for the formation of the four-membered ring (O(1)–C(2)–C(3)–C(4)) intermediate, since the orbital of O(1)–C(2) bond in $LUMO_{R1}$ is Π^*, but the orbital of C(3)=C(4) bond in $HOMO_{R2}$ (or $HOMO_{R3}$) is Π (Fig. 6). If the molecular orbital interactions are not concerned with orbital symmetries, Why two σ bonds (O(1)=C(4), C(2)–C(3)) cannot generate simultaneously via the transition state? Now all the questions are focused on the interaction between $LUMO_{R1}$ and $HOMO_{R2}$ (or $HOMO_{R3}$), so it is necessary to study why the formation of the C(2)–C(3) σ orbital is easier under the catalysis of BF_3.

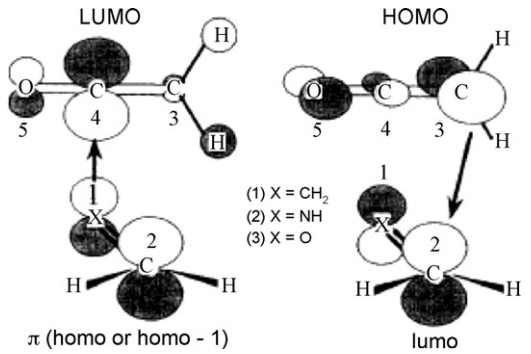

Fig. 5. The two one-centre frontier molecular orbital (FMO) interactions of the [2+2] cycloaddition [19d].

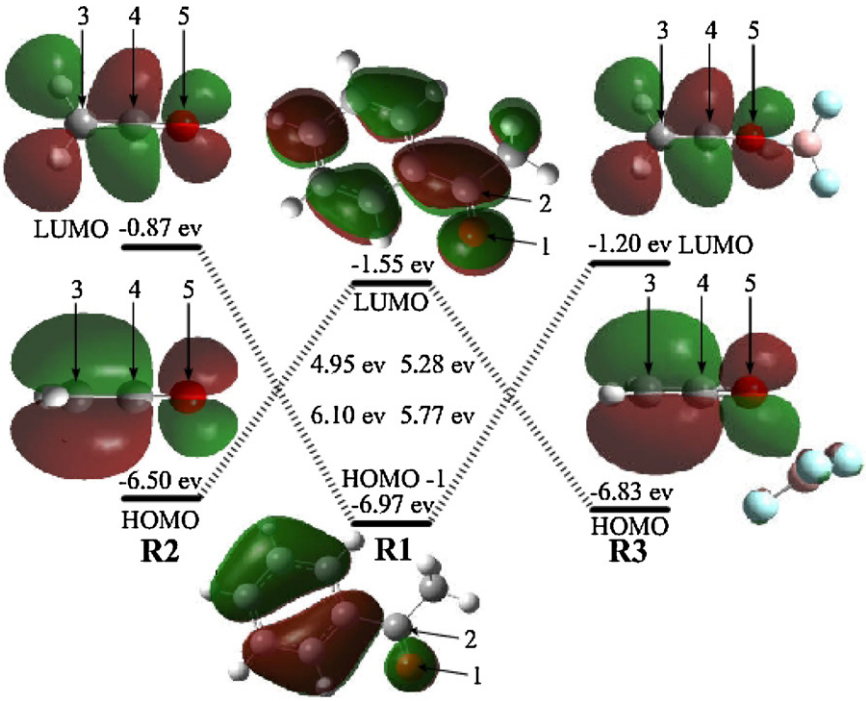

Fig. 6. The calculated frontier molecular orbitals of **R1**, **R2** and **R3** at the B3LYP/6-31G (d, p) level in CH_2Cl_2 solvent (unit: ev).

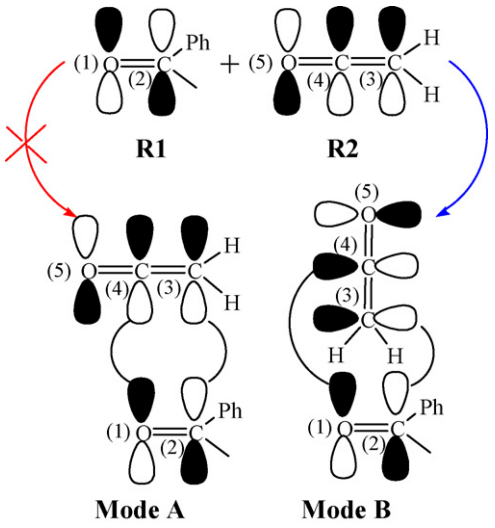

Fig. 7. The overlap modes A and B between the frontier molecular orbitals.

How does the C(2)–C(3) σ orbital generate? Noteworthy, from the IRC results of **TS1** (or **TS5**) we find that it is a one to one relationship between the frontier molecular orbitals of reactants and the frontier molecular orbitals of the four-memebered ring intermediates. For example, the $LUMO_{R1}$ can become the $LUMO_{M1}$ by the interaction with the Π orbital of C(3) and C(4) atoms via **TS1**, and the $HOMO_{R2}$ can become the $HOMO_{M1}$ by the interaction with the Π^* orbital of O(1) and C(2) atoms via **TS1**. And one can easily observe that the LUMO of **TS1** (or **TS5**) is the σ^* orbital localized on the C(2) and C(3) atoms, while the HOMO of **TS1** (or **TS5**) is the σ orbital localized on the C(2) and C(3) atoms. Hence, we can observe and trace the HOMO in the IRC points of **TS1** (or **TS5**) to understand how the $HOMO_{R2}$ (or $HOMO_{R3}$) becomes the C(2)–C(3) σ orbital by overlapping with the Π^* orbital as follows.

Several representative HOMOs of **TS1**'s IRC points are depicted in Fig. S1, which has been provided in Supplementary data. By comparison between Fig. 6 and Fig. S1, we can see that the shape and energy of HOMO in IRC-F-98 (Fig. S1) is the same as the $HOMO_{R2}$ (Fig. 6). As can be seen from Fig. S1, the Π^* orbital and the Π orbital of two reactants cannot overlap as a head to head mode (mode A, Fig. 7), but can overlap as a shoulder to head mode (mode B, Fig. 7) with **R1** getting close to **R2**. The energies of the HOMOs in the IRC points become higher and higher accompanied with overlapping by the shoulder to head mode. This phenomenon is so strange and it might explain why the energy of **TS1** is so high. Subsequently, accompanied by the gradual formation of O(1)–C(4) bond, the orbital of the O(1) atom overlaps with the orbital of C(4) atom less and less, and the shoulder to head overlap mode no longerexists. After IRC-R-20 (Fig. S1), only the orbital of the C(2) atom overlaps with the orbital of C(3) atom by one-center head to head overlap mode (mode C in Fig. 8), here the energies of the HOMOs in the IRC points become lower and lower accompanied with overlapping by the one-center head to head mode, and finally the four-membered ring intermediate **M1** generates. Noteworthy, the result of the Π orbital of $HOMO_{R2}$ overlapping with the Π^* orbital can only lead to the formation of C(2)–C(3) σ orbital, which is consistent with the study of Yamabe and co-workers [19d].

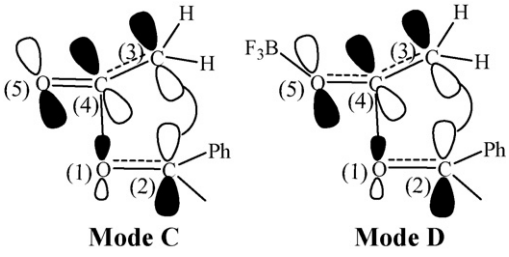

Fig. 8. The overlap modes C and D between the frontier molecular orbitals.

We have also observed all the orbital changes of **TS5** by IRC results. Notably, we find that the shapes of HOMOs in the IRC points are very similar to that of **TS1**, and the HOMOs are also the Π orbital of $HOMO_{R3}$ overlapped by the Π^* orbital of O(1) and C(2) atoms. The HOMO of **M3** and several representative HOMOs of the IRC points are shown in Fig. S2, which has also been provided in Supplementary data. The O(1)–C(4) bond has been generated in **M3**, and the orbital of the O(1) does not overlap with the orbital of the C(4) atom by shoulder to head mode. Now the head to head mode seems to be "symmetry-matched", here only the orbital of the C(2) overlaps with the orbital of the C(3) atoms by one-center head to head overlap mode, which is mode D in Fig. 8. And the energies of the HOMOs in the IRC points almost also become lower and lower accompanied with overlapping by the one-center head to head mode, at last, the four-membered ring intermediate **M4** has been obtained.

As concerned as above, it is easy to find that the head to head "symmetry-forbidden" overlap mode seems to become an one-center head to head "symmetry-matched" overlap mode after the formation of O(1)–C(4) bond. Because the "symmetry-mutated" only can appear after the formation of O(1)–C(4) bond, we think the path A in Schemes 2 and 3 certainly cannot lead to the β-lactones, which is in good agreement with the IRC results mentioned in the introduction, and this would provide a powerful evidence to disaffirm the path A in Schemes 2 and 3. Comparing the two different orbital overlap modes (mode B + C and D) and energy barriers, we can conclude that the head to head overlap mode should be more energy favorable than the shoulder to head overlap mode, and the BF_3 should lower the energy barrier mainly by changing the overlap mode rather than effecting the orbital symmetries and energy gaps between the reactants' frontier molecular orbitals.

4. Conclusions

This work has studied three possible reaction channels of the title reaction with **P1**, **P2** and **P** as the products at the B3LYP/6-31G (d, p) level of theory in CH_2Cl_2 solvent using IEF-PCM. In all the three reaction channels, the energy barriers of two catalyzed channels (channels 2 and 3) are much lower than the non-catalyzed channel (channel 1), and reaction channel 2 is most energy favorable among the three reaction channels, hence we think it should be the main reaction channel of the title reaction, and the product **P** would be the main product, which is in good agreement with the experimental results.

The method of tracing the frontier molecular orbitals of IRC has been employed to study how the frontier molecular orbitals overlap and what the role of BF_3 is. The concerted reaction has become a stepwise reaction and the energy barrier of rate-determining step has been largely lowered under the catalysis of Lewis acid BF_3, which is mainly due to the change on the overlap mode rather than the orbital symmetries and energy gaps between the frontier molecular orbitals.

Acknowledgment

The work described in this paper was supported by the National Natural Science Foundation of China (No. 20873126).

Appendix A. Supplementary data

Supplementary data associated with this article can be found, in the online version, at doi:10.1016/j.molcata.2010.04.005.

References

[1] (a) M.C. Willis, J. Chem. Soc. Perkin Trans. 1 (1999) 1765–1784;
(b) E. García-Urdiales, I. Alfonso, V. Gotor, Chem. Rev. 105 (2005) 313–354.
[2] A. Fryszkowska, M. Komar, D. Koszelewski, R. Ostaszewski, Tetrahedron: Asymmetr. 17 (2006) 961–966.
[3] S.P. Keen, C. Cowden, J. Org. Chem. 70 (2005) 1771–1779.
[4] R. Shintani, G.C. Fu, Angew. Chem., Int. Ed. 41 (2002) 1057–1059.
[5] Y. Chen, S.-K. Tian, L. Deng, J. Am. Chem. Soc. 122 (2000) 9542–9543.
[6] (a) W.T. Smith, R.W. Shelton, J. Am. Chem. Soc. 76 (1954) 2731–2732;
(b) W.T. Smith, P.G. Kort, J. Am. Chem. Soc. 72 (1950) 1877–1878.
[7] M.F.A. Adamo, V.R. Konda, D. Donati, P. Sarti-Fantoni, T. Torroba, Tetrahedron 63 (2007) 9741–9745.
[8] H. Matsunaga, K. Ikeda, K. Iwamoto, Y. Suzuki, M. Sato, Tetrahedron Lett. 50 (2009) 2334–2336.
[9] A. Pommier, J.-M. Pons, Synthesis (1993) 441–459.
[10] A. Pommier, J.-M. Pons, Synthesis (1995) 729–744.
[11] G.S. Zaitseva, N.G. Vinokurova, Y.I. Baukov, Zh. Obshch. Khim. 45 (1975) 1398.
[12] G.S. Zaitseva, L.I. Vasil'eva, N.G. Vinokurova, O.A. Safronova, Y.I. Baukov, Zh. Obshch. Khim. 48 (1978) 1363–1368.
[13] K. Maruoka, A.B. Concepcion, H. Yamamoto, Synlett (1992) 31–32.
[14] A.B. Concepcion, K. Maruoka, H. Yamamoto, Tetrahedron 51 (1995) 4011–4020.
[15] J.-M. Pons, A. Pommier, J. Lerpiniere, P. Kocienski, J. Chem. Soc., Perkin Trans. 1 (1993) 1549–1551.
[16] A. Pommier, J.-M. Pons, P.J. Kocienski, L. Wong, Synthesis (1994) 1294–1300.
[17] A. Pommier, J.-M. Pons, P.J. Kocienski, J. Org. Chem. 60 (1995) 7334–7339.
[18] X.-N. Wang, P.-L. Shao, H. Lv, S. Ye, Org. Lett. 11 (2009) 4029–4031.
[19] (a) D.C. Fang, X.Y. Fu, Chin. Chem. Lett. 3 (1992) 367–368;
(b) B. Lecea, A. Arrieta, G. Roa, J.M. Ugalde, F.P. Cossio, J. Am. Chem. Soc. 116 (1994) 9613–9619;
(c) B. Lecea, A. Arrieta, X. Lopez, J.M. Ugalde, F.P. Cossio, J. Am. Chem. Soc. 117 (1995) 12314–12321;
(d) S. Yamabe, T. Minato, Y. Osamura, J. Chem. Soc., Chem. Commun. (1993) 450–452;
(e) S. Yamabe, K. Kuwata, T. Minato, Theor. Chem. Acc. 102 (1999) 139–146;
(f) X. Wang, K.N. Houk, J. Am. Chem. Soc. 112 (1990) 1754–1756.
[20] (a) J.-M. Pons, A. Pommier, M. Rajzmann, D. Liotard, J. Mol. Struct. (Theochem) 313 (1994) 361–364;
(b) J.-M. Pons, M. Oblin, A. Pommier, M. Rajzmann, D. Liotard, J. Am. Chem. Soc. 119 (1997) 3333–3338.
[21] (a) J. Zhao, M.-S. Tang, D.-H. Wei, C.-F. Zhao, W.-J. Zhang, H.-M. Wang, Int. J. Quantum Chem. 109 (2009) 1036–1044;
(b) D.-H. Wei, M.-S. Tang, J. Zhao, L. Sun, W.-J. Zhang, C.-F. Zhao, S.-R. Zhang, H.-M. Wang, Tetrahedron: Asymmetr. 20 (2009) 1020–1026;
(c) L. Sun, M.-S. Tang, H.-M. Wang, D.-H. Wei, L.-L. Liu, Tetrahedron: Asymmetr. 19 (2008) 779–787;
(d) D.-H. Wei, M.-S. Tang, H.-M. Wang, S. Li, J. Zhao, C.-F. Zhao, Acta Chim. Sinica 66 (2008) 321–324;
(e) D.-H. Wei, M.-S. Tang, J. Phys. Chem. A 113 (2009) 11035–11041;
(f) J.-Y. Yuan, X.-C. Liao, H.-M. Wang, G.-Y. Yang, M.-S. Tang, J. Phys. Chem. B 113 (2009) 1418–1422.
[22] (a) S. Fomine, J.V. Ortega, M.A. Tlenkopatchev, Organometallics 24 (2005) 5696–5701;
(b) S. Fomine, S.M. Vargas, M.A. Tlenkopatchev, Organometallics 22 (2003) 93–99;
(c) S. Fomine, J.V. Ortega, M.A. Tlenkopatchev, J. Mol. Catal. A: Chem. 263 (2007) 121–127;
(d) X. Zheng, P. Blowers, J. Mol. Catal. A: Chem. 246 (2006) 1–10;
(e) X. Zheng, P. Blowers, J. Phys. Chem. A 110 (2006) 2455–2460;
(f) X. Zheng, P. Blowers, J. Phys. Chem. A 109 (2005) 10734–10741;
(g) M. Freccero, R. Gandolfi, M. Sarzi-Amade, A. Rastelli, J. Org. Chem. 65 (2000) 8948–8959;
(h) M. Freccero, R. Gandolfi, M. Sarzi-Amade, A. Rastelli, J. Org. Chem. 65 (2000) 2030–2042;
(i) M. Freccero, R. Gandolfi, M. Sarzi-Amade, A. Rastelli, J. Org. Chem. 64 (1999) 3853–3860;
(j) M. Freccero, R. Gandolfi, J. Org. Chem. 70 (2005) 7098–7106;
(k) M. Freccero, R. Gandolfi, M. Sarzi-Amadè, A. Rastelli, J. Org. Chem. 69 (2004) 7479–7485;
(l) S. Yamabe, S. Yamazaki, J. Org. Chem. 72 (2007) 3031–3041;
(m) N. Tsuchida, H. Satou, S. Yamabe, J. Phys. Chem. A 111 (2007) 6296–6303.
[23] A.D. Becke, J. Chem. Phys. 98 (1993) 5648–5652.
[24] C. Lee, W. Yang, R.G. Parr, Phys. Rev. B 37 (1988) 785–789.
[25] B. Miehlich, A. Savin, H. Stoll, H. Preuss, Chem. Phys. Lett. 157 (1989) 200–206.
[26] V. Barone, M. Cossi, J. Phys. Chem. A 102 (1998) 1995–2001.
[27] B. Mennucci, J. Tomasi, J. Chem. Phys. 106 (1997) 5151–5158.
[28] C. Gonzalez, H.B. Schlegel, J. Chem. Phys. 90 (1989) 2154–2161.
[29] C. Gonzalez, H.B. Schlegel, J. Phys. Chem. 94 (1990) 5523–5527.
[30] M.J. Frisch, G.W. Trucks, H.B. Schlegel, G.E. Scuseria, M.A. Robb, J.R. Cheeseman, J.A. Montgomery Jr., T. Vreven, K.N. Kudin, J.C. Burant, J.M. Millam, S.S. Iyengar, J. Tomasi, V. Barone, B. Mennucci, M. Cossi, G. Scalmani, N. Rega, G.A. Petersson, H. Nakatsuji, M. Hada, M. Ehara, K. Toyota, R. Fukuda, J. Hasegawa, M. Ishida, T. Nakajima, Y. Honda, O. Kitao, H. Nakai, M. Klene, X. Li, J.E. Knox, H.P. Hratchian, J.B. Cross, C. Adamo, J. Jaramillo, R. Gomperts, R.E. Stratmann, O. Yazyev, A.J. Austin, R. Cammi, C. Pomelli, J.W. Ochterski, P.Y. Ayala, K. Morokuma, G.A. Voth, P. Salvador, J.J. Dannenberg, V.G. Zakrzewski, S. Dapprich, A.D. Daniels, M.C. Strain, O. Farkas, D.K. Malick, A.D. Rabuck, K. Raghavachari, J.B. Foresman, J.V. Ortiz, Q. Cui, A.G. Baboul, S. Clifford, J. Cioslowski, B.B. Stefanov, G. Liu, A. Liashenko, P. Piskorz, I. Komaromi, R.L. Martin, D.J. Fox, T. Keith, M.A. Al-Laham, C.Y. Peng, A. Nanayakkara, M. Challacombe, P.M.W. Gill, B. Johnson, W. Chen, M.W. Wong, C. Gonzalez, J.A. Pople, Gaussian 03, Revision C. 02, Gaussian, Inc., Wallingford, CT, 2004.